Electric-field induced spin textures in a superlattice with Rashba and Dresselhaus spin-orbit coupling

D. V. Khomitsky*
Department of Physics, University of Nizhny Novgorod, 23 Gagarin Avenue, 603950 Nizhny Novgorod, Russian Federation
(Received 28 May 2008; revised manuscript received 10 February 2009; published 4 May 2009)

The dc charge current, field induced spin polarization, and spin textures are studied in the one-dimensional gated superlattice with both fixed and varying Rashba and Dresselhaus contributions to spin-orbit coupling. It is found that a spin component with zero mean value can demonstrate nonvanishing field induced spin texture in a superlattice cell which can be probed experimentally, with the highest amplitudes achievable in an interval of comparable Rashba and Dresselhaus terms. The consideration of the finite parameters for collision rate and temperature is found to be nondestructive for the calculated current and spin characteristics depending on all states below the Fermi level.

DOI: 10.1103/PhysRevB.79.205401 PACS number(s): 73.21.Cd, 72.25.Dc, 73.50.Fq

I. INTRODUCTION

The spin polarization of charge carriers in nanostructures is an important issue for both electronics and new field of condensed-matter physics known as spintronics.[1,2] One of the problems being actively studied nowadays is the control of spin (in general, magnetic moment) degrees of freedom for the carriers participating in the electron transport, optical, magnetization, etc., phenomena. The classical and approved way to achieve this goal is the application of external magnetic fields which is successfully used both in fundamental experiments and in commercial device structures. With all its advantages the application of external magnetic field is not always desirable for the technological purposes. Hence, alternative methods of spin control are interesting for both fundamental and applied issues. One of them is the consideration of the spin-orbit (SO) coupling in those semiconductor nanostructures where it can produce measurable and potentially usable effects. One type of the SO coupling in heterostructures is the Rashba coupling[3] coming from the structure inversion asymmetry (SIA) of confining potential and effective-mass difference. It is important for the experimental purposes that the value of Rashba coupling strength can be tuned by the external gate voltage[4] and reaches the value of 2×10^{-11} eV m in InAs-based structures[5] with two-dimensional electron gas (2DEG) which makes its influence to be quite substantial. Furthermore, the Dresselhaus term[6] originating due to the bulk inversion asymmetry (BIA) is also present in the most commonly used types of heterostructures. The ratio between the Rashba term with strength α and Dresselhaus term with strength β can be as small as $\alpha/\beta=1.6$ which was reported in the photocurrent experiments.[7] Hence, it seems reasonable to include both Rashba and Dresselhaus terms for more accurate description of the SO coupling in these structures. The inclusion of both terms will be further justified if one can find an effect which is sensitive to the particular form of the SO coupling.

In the great variety of spin-dependent properties the problem of field induced carrier polarization which accompanies the charge current flow is one of the central ones. Since the pioneer work by Datta and Das[8] on the concept of spin field-effect transistor it attracts considerable attention, and one of the key issues is the spin polarization induced by an external electric field in the presence of the SO coupling.[9–11] Apart from the great variety of the results on the challenging problem of spin current, one can mention the calculations of spin susceptibilities,[12] the spin polarizations in a bar[13–15] or in the T-shaped conductor,[16] the interplay between spin and Hall charge current,[17] the spin accumulation in a quantum wire device,[18] the pumping of charge current by spin dynamics,[19] the dynamics of localized spins coupled to the conduction electrons,[20] the injected current-control[21] and detection[22] of spin accumulation,[23,24] the spin Gunn effect,[25] and a recent proposal of the spin current diode.[26] Another important problem is a possible influence of random nanosize domains of the SO coupling formed due to the imperfections of the structure,[27] which can give rise to the spatially nonuniform character of SO terms leading to the electron-spin precession[28] and the effects referred to the field of spin optics.[29]

One of possible ways to create a nonuniform spin distribution in a heterostructure is to apply a metal-gated superlattice with tunable amplitude of electric potential to the 2DEG with the SO coupling. It was shown by Kleinert *et al.*[23] that in the presence of Rashba SO coupling the external electric field yields an enhanced spin polarization in a superlattice with a single spin-split band. In addition to the total polarization of the sample, one can be interested in calculating the local polarization (or spin density) at the point of a real space which may be actually probed by a detector. It is known that the states with inhomogeneous distribution of spin density can exist and, which is important, can have long spin-relaxation time.[30] It was shown that such states can be found in a one-dimensional (1D) superlattice with Rashba SO coupling demonstrating a nonuniform distribution of spin density for a given state $\mathbf{k}$, i.e., showing a spin texture.[31] Of course, under the equilibrium conditions the contributions to the local spin density from all states below Fermi level cancel each other since the populations of the $\mathbf{k}$ and $-\mathbf{k}$ states with the opposite spin projections in a system without magnetic order are equal. However, in the presence of symmetry breakup during scattering[32] or in a nonequilibrium condition created by an external radiation,[33] one can observe various and controllable spin textures along the superlattice cell.

Hence, it seems also promising to look at the spin polarizations of the charge current and the spin textures created by an external dc field applied to the superlattice.

In the present paper we study the dc, the spin polarization, and the spin textures in the 1D gated superlattice with simultaneous presence of both Rashba and Dresselhaus SO terms. The shape of spin textures is calculated as a function of the applied electric field for fixed values of Rashba and Dresselhaus SO amplitudes α and β and also as a function of α/β ratio at fixed electric field and in the interval of α/β covering a rather wide range of semiconductor materials. We consider the finite parameters of collision rate and temperature which appear to be nondestructive for the calculated current and spin characteristics depending on all states below the Fermi level. The knowledge of field induced spin textures in addition to the spin polarization and charge current may be instructive for both fundamental and applied issues of low-dimensional semiconductor structures with strong SO coupling. It will be seen that the principal results of the paper regarding the generation of spin textures in a superlattice can be obtained in a rather elementary model. In this model a simple stationary kinetic equation is considered with a constant relaxation time and all the calculations of the physical quantities based on the knowledge of Bloch spinors and the miniband spectrum while keeping in mind that a more general formalism of spin-density matrix can also be applied for more detailed studies.[9–11]

This paper is organized as follows. In Sec. II we briefly describe quantum states and spin polarizations in the minibands of a superlattice with Rashba and Dresselhaus SO coupling. In Sec. III we write down the kinetic equation for the distribution function in the presence of the dc electric field and solve it numerically. The distribution function is used for obtaining the charge current and the mean spin projections as well as the spin textures. In Sec. IV we calculate and discuss the spin textures for both fixed Rashba and Dresselhaus amplitudes and for varying α/β ratio. The concluding remarks are given in Sec. V.

II. QUANTUM STATES IN SO SUPERLATTICE

In this section we shall briefly describe the quantum states of 2DEG with Rashba and Dresselhaus SO coupling subjected to a 1D periodic superlattice potential. A model involving only the Rashba contribution to the SO coupling and a superlattice potential has been derived previously[31] and applied to the problem of scattering[32] and optical excitation of spin textures.[33] The Hamiltonian is the sum of the 2DEG kinetic-energy operator in a single size quantization band with effective mass m, the Rashba and Dresselhaus SO terms with amplitudes α and β, respectively, and the periodic electrostatic potential of the 1D superlattice:

$$\hat{H} = \frac{\hat{p}^2}{2m} + \alpha(\hat{\sigma}_x\hat{p}_y - \hat{\sigma}_y\hat{p}_x) + \beta(\hat{\sigma}_y\hat{p}_y - \hat{\sigma}_x\hat{p}_x) + V(x), \quad (1)$$

where $\hbar=1$ and the periodic potential is chosen in the simplest form, $V(x)=V_0\cos 2\pi x/a$, where a is the superlattice period and the amplitude V_0 can be tuned by the gate voltage. The eigenstates of Hamiltonian (1) are two-component Bloch spinors with eigenvalues labeled by the quasimomentum k_x in a one-dimensional Brillouin zone $-\pi/a \le k_x \le \pi/a$, the momentum component k_y, and the miniband index m:

$$\psi_{m\mathbf{k}} = \sum_{\lambda n} a^m_{\lambda n}(\mathbf{k}) \frac{e^{i\mathbf{k}_n\mathbf{r}}}{\sqrt{2}} \begin{pmatrix} 1 \\ \lambda e^{i\theta_n} \end{pmatrix}, \quad \lambda = \pm 1. \quad (2)$$

Here $\mathbf{k}_n = \mathbf{k} + n\mathbf{b} = (k_x + \frac{2\pi}{a}n, k_y)$ and $\theta_n = \arg[\alpha k_y + \beta k_{nx} - i(\alpha k_{nx} + \beta k_y)]$. The energy spectrum of Hamiltonian (1) consists of pairs of spin-split minibands. The spacing between two minibands in a pair is mainly determined by the SO parameters α and β, while the miniband widths and the gaps in the spectrum are on the order of the superlattice potential amplitude V_0. An example of the energy spectrum is shown in Fig. 1 for the four lowest minibands in the InAs-based 1D superlattice with Rashba parameter $\alpha=2\times10^{-11}$ eV m plus the Dresselhaus SO term with the amplitude $\beta=1.25\times10^{-11}$ eV m. Here the ratio $\alpha/\beta=1.6$ corresponds to the one measured in the photocurrent experiments on InAs-based structures.[7] The cited experiments have shown that the ratio α/β for the most widely used two-dimensional (2D) structures varies from 1.5 for GaAs/AlGaAs and 1.6 for InAs/InAlAs quantum wells to 7.6 in a single GaAs/AlGaAs heterojunction. One can see from Table I of Ref. 7 that none of the samples has shown a negligible impact of the Dresselhaus term and hence this contribution should be included in the SO part of the Hamiltonian. The other parameters are the InAs electron effective mass $m=0.036m_0$, the superlattice period $a=60$ nm, and the amplitude of the periodic potential $V_0=10$ meV. It should be noted that the spectrum in Fig. 1 is limited to the first Bril-

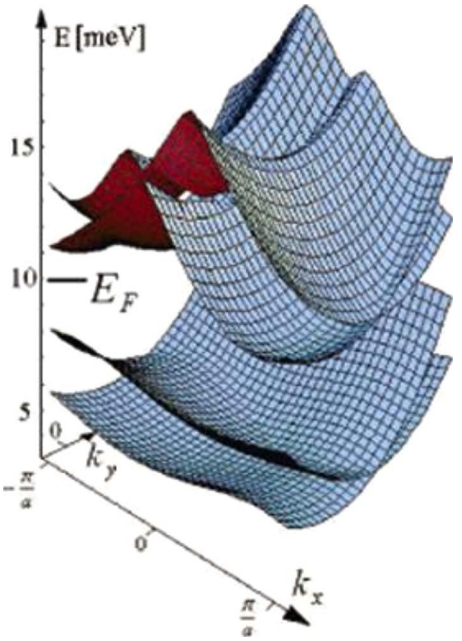

FIG. 1. (Color online) Energy spectrum of four lowest minibands in the InAs 1D superlattice with Rashba SO term $\alpha=2\times10^{-11}$ eV m and the Dresselhaus term $\beta=1.25\times10^{-11}$ eV m. The other parameters are the electron effective mass $m=0.036m_0$, the superlattice period and amplitude $a=60$ nm, and $V_0=10$ meV.

louin zone of the superlattice in the k_x direction, while the cutoff in the k_y direction is shown only to keep the limits along k_x and k_y comparable. The minibands in Fig. 1 have an inversion symmetry $E(\mathbf{k})=E(-\mathbf{k})$ but they do not have an additional symmetry with respect to the change $k_{x,y}\rightarrow -k_{x,y}$ if both Rashba and Dresselhaus terms are present. This feature is very important for the symmetry analysis of the present structure as well as for the induced spin textures since the absence of the additional symmetry plane perpendicular to the y axis allows the generation of S_x and S_z components of spin density for the x-oriented electric field, as we shall see below in Sec. IV. Another argument for the consideration of the lowest available symmetry of the SO term is the possible influence of random nanosize domains of the SO coupling which can be present due to the imperfections of the structure.[27]

An external electric field changes the occupation distribution in the reciprocal space and thus it may produce noncompensated impacts from states with different quasimomenta to the local spin densities from the symmetrical points in $\mathbf{k}$ space. Hence, it is instructive to take a look at the spin polarization described by a vector field $(\sigma_x(\mathbf{k}),\sigma_y(\mathbf{k}))$ in the (k_x,k_y) plane. Each of the mean spin projections is given by

$$\sigma_i(\mathbf{k})=\langle\psi_\mathbf{k}|\hat{\sigma}_i|\psi_\mathbf{k}\rangle \tag{3}$$

and is calculated for each miniband separately with a given $\psi_\mathbf{k}$. The spin vector field is two dimensional since for both Rashba and Dresselhaus terms the mean value of σ_z is zero. We are interested in the topological structure of vector field (3) in each miniband since it can provide a justified estimation about the measurable local spin density which can be induced by an external electric field.

In Fig. 2 the vector field $(\sigma_x(\mathbf{k}),\sigma_y(\mathbf{k}))$ is shown schematically for two lowest superlattice minibands with the same parameters as in Fig. 1 with both Rashba and Dresselhaus SO terms. In can be seen from Figs. 1 and 2 that the periodicity of the superlattice along x leads to the same property in the $\mathbf{k}$ space for both energy and spins with the reciprocal lattice vector $(2\pi/a,0)$. In each miniband the relation

$$\vec{\sigma}(\mathbf{k})=-\vec{\sigma}(-\mathbf{k}) \tag{4}$$

is satisfied, so in equilibrium at each point in the real space the contribution $\vec{\sigma}(\mathbf{k})$ is compensated for by the term $-\vec{\sigma}(-\mathbf{k})$, leaving the sample nonmagnetic. If an external electric field is applied along x direction, relation (4) is no longer satisfied, and one can find a nonzero spin accumulation at the edges of the sample. In the next section we shall calculate this quantity in the presence of the electric field oriented parallel to the superlattice direction x for Rashba plus Dresselhaus types of SO coupling.

III. CHARGE CURRENT AND MEAN SPIN VALUES

A. Kinetic equation for the distribution function

The field induced distribution of spin density and the charge current can be calculated with the nonequilibrium stationary distribution function $f_m(\mathbf{k})$ in the miniband m which depends only on the momentum if the stationary and uniform

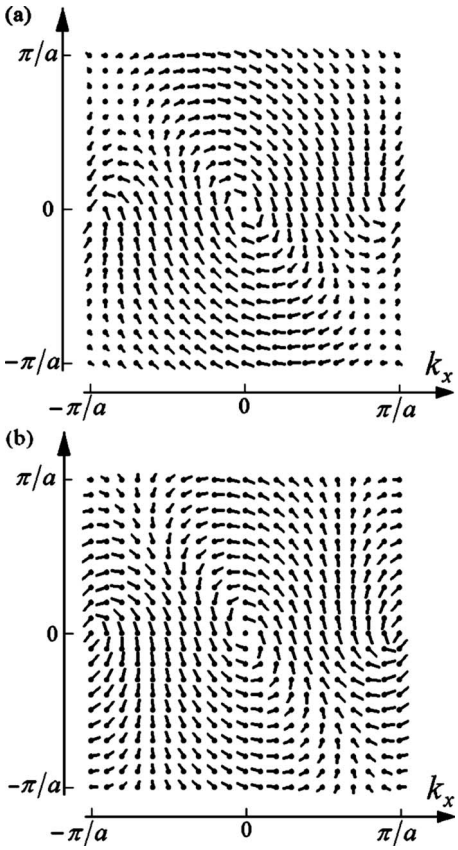

FIG. 2. Spin polarization [the origin of vector $\vec{\sigma}(\mathbf{k})$ is marked by black circles] (a) in two lowest miniband and (b) in the next miniband of spectrum in Fig. 1 with the presence of both Rashba and Dresselhaus SO coupling terms with the amplitude ratio $\alpha/\beta=1.6$.

external electric field E_x is applied along the x direction of the superlattice. We shall neglect possible nonuniform character of the distribution function in a real space arising due to the strong nonlinearity at high electric field and resulting to the current and the charge domains of instability. Still, our calculations will include the electric fields high enough to see the nonlinear dependence of both the induced spin densities and the current on the applied field strength.

In the collision frequency approximation the kinetic equation for $f_m(\mathbf{k})$ under the conditions described above has a simple form,

$$eE_x\frac{\partial f_m(\mathbf{k},E_x)}{\partial k_x}=-\nu[f_m(\mathbf{k},E_x)-F_m(\mathbf{k})], \tag{5}$$

where ν is the collision rate and $F_m(\mathbf{k})=1/(1+\exp\{[E_m(\mathbf{k})-\mu]/k_BT\})$ is the Fermi equilibrium distribution function in the mth miniband. In the following we shall assume that $T=77$ K and $\nu=10^{12}$ s^{-1}, which corresponds to the thermal and collision broadenings of 6.6 and 3.9 meV, respectively. The position of the Fermi level can be tuned by the gate voltage and we assume $E_F=10$ meV counted from the bottom of the electron size quantization band. Such broadening parameters are typical in the experiments and produce significant smearing of the SO-split miniband structure shown

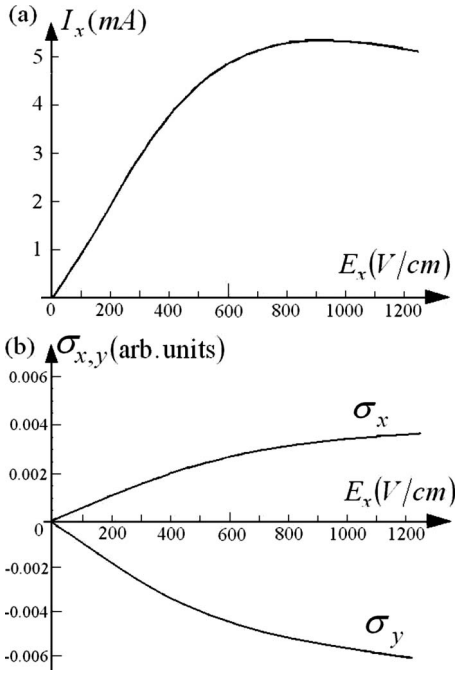

FIG. 3. (a) Charge current and (b) mean spin projections induced by the electric field in the superlattice with Rashba plus Dresselhaus SO terms. The current in (a) is calculated for a 1×1 mm^2 structure with electron density $n=10^{12}$ cm^{-2} and with all other parameters as in Fig. 1.

in Fig. 1. However, the charge current, the mean spin values, and the local spin density are determined by the contributions from all occupied states which makes it survivable under this scale of broadening. By substituting the dispersion relation $E_m(\mathbf{k})$ obtained in the previous section for each miniband, kinetic equation (5) can be solved directly for the given strength of the electric field E_x, allowing one to find the charge current and the spin density.

B. Mean charge current and spin

The application of an external electric field generates the charge current through the superlattice. In the presence of the electric field E_x applied along x, the charge current $J_x(E_x)$ and the mean spin values $\sigma_i(E_x)$ can be calculated directly after obtaining the distribution function from Eq. (5):

$$J_x(E_x) = e\sum_{m,\mathbf{k}} \langle \psi_{m\mathbf{k}}|\hat{v}_x|\psi_{m\mathbf{k}}\rangle f_m(\mathbf{k},E_x), \tag{6}$$

$$\sigma_i(E_x) = \sum_{m,\mathbf{k}} \langle \psi_{m\mathbf{k}}|\hat{\sigma}_i|\psi_{m\mathbf{k}}\rangle f_m(\mathbf{k},E_x), \tag{7}$$

where $\hat{v}_i=\partial\hat{H}/\partial k_i$, and the summation is performed over all minibands m and all values of $-\pi/a\le k_x\le\pi/a$ and k_y, respectively. The results are shown in Fig. 3(a) for the charge current and in Fig. 3(b) for the mean spin values. The current in Fig. 3(a) is calculated for a 1×1 mm^2 structure with 2DEG concentration $n=10^{12}$ cm^{-2} and with all other parameters as for the band structures in Fig. 1. It can be seen from Fig. 3(a) that the low-field Ohmic resistance of such structure is about 13 kΩ. Another well-known feature of the plots in Fig. 3 is the progressive nonlinear dependence of the maximum current and spin amplitude which can be seen at high electric field (greater than 500 V/cm). Such nonlinearity is common for all field induced quantities in superlattices and is significant when the Stark frequency $\Omega=|e|E_xa/\hbar$ becomes comparable with the collision frequency ν.

It is known that in the presence of Rashba SO term the only nonvanishing component of the E_x electric-field induced accumulated spin is σ_y.[23] In the presence of both Rashba and Dresselhaus terms the σ_x component can also be nonzero, as evident by looking onto the topology of the spin vector field in Fig. 2. This topological aspect is confirmed by the calculations of mean spin value dependencies on the electric field which are shown in Fig. 3(b). One can see that σ_x and σ_y can have an equal magnitude as long as the Dresselhaus term is comparable to the Rashba term. Thus, the consideration of both Rashba and Dresselhaus terms seems to be important for the calculation of nonvanishing spin components measured experimentally. Another spin-related quantity that we shall discuss below and which is actually measured in the experiments is the local spin density in a real space determined by all states below the Fermi level. We shall see that these spin densities can be spatially nonuniform in the presence of the superlattice potential.

IV. SPIN TEXTURES

Since the SO coupling is present, the spin polarization of charge carriers may also take place, resulting in a spin accumulation in a superlattice.[23] The spin-related quantity which can actually be probed by a tip in the experiment or possibly utilized in a spintronic nanostructure device is the local spin density in a real space, which manipulation is one of the primary goals of spintronics. The local change in the spin density is often referred to the conception of a spin current which permanently attracts a considerable attention of researchers[12,24,34–36] (only few from a great number of published papers on the spin current are cited here as an example), and where the different definitions have been proposed. Taking into consideration the goals of the present paper, one should mention that the experimental studies of the spin current phenomena are presently focused on the observation of spin accumulation. Indeed, one can observe an equal change in local spin density caused by two different processes: the first one is the transport of spin-polarized charge carriers, while the second one is the local "rotation" of spins which is not always accompanied by the carrier transfer. In both cases the actually measured observable is the local spin density which change, as we see, does not strictly require involving the conception of spin current. The problem of the spin current definition remains to be one of the hottest topics on spintronics since the work of Rashba,[37] where the possibility of the existence of spin currents even in the equilibrium has been demonstrated. The different possibilities of local spin evolution are reflected also in the nonconservation of the spin in terms of the continuity equation $\partial S_i/\partial t+(\nabla\cdot\mathbf{J}_i)=T_i$. If the spin current density is defined as $J_i^j=\mathrm{Re}[\psi^\dagger\frac{1}{2}\{v_j,\sigma_i\}\psi]$, then one has to introduce the torque

density $T_i=\mathrm{Re}[\psi^\dagger \frac{1}{i}[\sigma_i,H]\psi]$ in the right side of the continuity equation. It was shown that this equation takes the usual form with zero in the right side if another definition $J_i^j = \frac{d}{dt}(x^j\sigma_i)$ of spin current is considered.[35] The proper and uniform definition of spin current based on the measurable quantities is still under discussion, and the goal of the present paper is the local measurable spin density rather than the spin current. Hence, below we shall focus on the electric-field induced local spin density which is nonuniform in the superlattice cell and thus can be referred to as the spin texture. It should be stressed that this texture accompanies the charge current and thus provides the information about the tunable spin polarization of the electrical current, which is of big importance for possible device applications.

A. Fixed α/β and variable electric field

The Rashba and Dresselhaus SO terms in a Hamiltonian of the free particle produce a spin polarization for the plane-wave spinor $\psi_{\mathbf{k}}$ with a given $\mathbf{k}$ which has a uniform spin-density distribution in the real space. If an additional superlattice potential is applied, the spin density for $\psi_{m\mathbf{k}}$ in the mth miniband becomes nonuniform and forms the spin texture.[31] In the equilibrium conditions the spin densities from all states below E_F cancel each other, which leads to zero spin density in any point of the real space. If the equilibrium is destroyed by an external electric field, one can expect to measure not only the nonzero spin accumulation[23] but also the local spin density which varies along the superlattice cell and forms variable spin textures which shape can be modified by manipulating the system parameters.

In this subsection we are interested in calculating the spin density $S_i(x,E_x)$ along the superlattice cell as a function of the electric-field strength E_x. If the electric field is applied along x, then the density depends only on x in the real space since in the y direction the system is totally homogeneous. After obtaining the distribution function from Eq. (5), one can write

$$S_i(x,E_x) = \sum_{m,\mathbf{k}} (\psi^\dagger_{m\mathbf{k}}\hat{\sigma}_i\psi_{m\mathbf{k}}) f_m(\mathbf{k},E_x), \tag{8}$$

where the summation and integration are performed over all minibands m and all values of $-\pi/a \le k_x \le \pi/a$ and k_y, respectively. The results can be presented in a form of a three-dimensional (3D) plot showing each of the spin-density components S_i separately as a function of the position x inside the superlattice cell and the electric-field strength E_x.

In Fig. 4 we show the field induced spin textures in a 2DEG for two limiting cases with $\beta=0$ and $\alpha=0$ as well as for the fixed Rashba-to-Dresselhaus ratio $\alpha/\beta=1.6$, taking all other system parameters as in Fig. 1. The plots in Fig. 4 and below in Fig. 5 show each component of spin [$S_x(x)$ in panel (a), $S_y(x)$ in panel (b), and $S_z(x)$ in panel (c)] separately on the vertical axis calculated as a $z=f(x,y)$ function of the position x in a superlattice cell (x axis) and of the applied electric field (E_x axis in Fig. 4) or of the α/β ratio (α/β axis in Fig. 5). At zero electric field the structure is maintained in

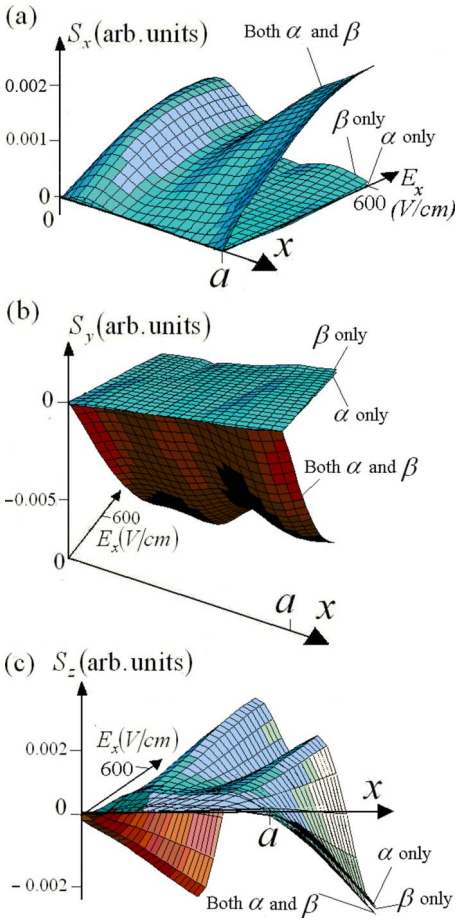

FIG. 4. (Color online) Electric-field dependence of spin texture, (a) x component, (b) y component, and (c) z component shown in one superlattice cell $0 \le x \le a$ for the field interval $0 \le E_x \le E_{\max}$. The textures for two limiting cases with $\beta=0$ and $\alpha=0$ as well as for the fixed Rashba-to-Dresselhaus ratio $\alpha/\beta=1.6$ corresponding to InAs-based structure are shown. The temperature $T=77$ K, the collision rate $\nu=10^{12}$ s^{-1}, and all other parameters are the same as in Fig. 1.

the thermodynamic equilibrium with equal population of the $\mathbf{k}$ and $-\mathbf{k}$ states in the reciprocal space having the opposite spin projections. Thus, without the electric-field induced imbalance of this population, the structure is not expected to demonstrate nonzero spins in any point of the real space; i.e., the spin textures in our system have a nonequilibrium origin.

The most striking feature of spin textures in Fig. 4 is the big amplitude difference of the field induced spin texture components S_x and S_y for limiting cases $\beta=0$ and $\alpha=0$ and for a general case $\alpha/\beta=1.6$, while the S_z amplitude is rather unaffected by the α/β variations. The explanation of this effect comes from the symmetry considerations as well as from the analysis of the SO superlattice subband energy spectrum which is presented schematically in Fig. 6. First of all, it should be mentioned that in the superlattice with SO coupling the energy subbands always come in pairs. Inside each pair the dispersion surfaces are relatively weakly split by the SO coupling (see Fig. 1) and their contributions to the

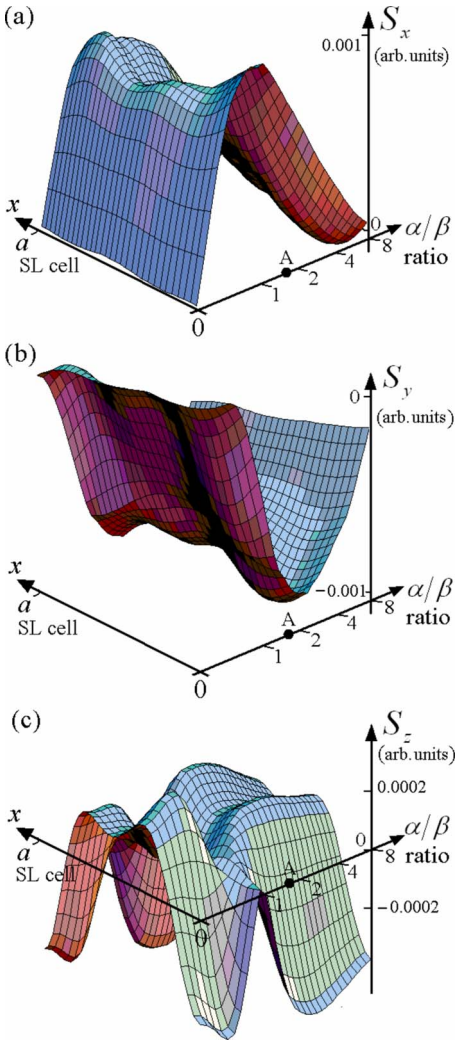

FIG. 5. (Color online) The dependence on Rashba-to-Dresselhaus parameter ratio α/β of the spin textures in the superlattice cell $0 \le x \le a$ for (a) x component, (b) y component, and (c) z component induced at fixed electric field $E_x = 50$ V/cm. Point "A" corresponds to the example of InAs-based structure with $\alpha/\beta = 1.6$ considered above. All other parameters are the same as in Figs. 4 and 1. The electric-field induced spin textures have the biggest amplitudes in a region of comparable Rashba and Dresselhaus contributions to spin-orbit coupling.

induced spin textures are in general of opposite signs (see Fig. 2). In order to illustrate this we plot in Fig. 6(a) a very simple schematic view of mean spin alignment in the **k** space for two SO-split superlattice subbands for pure Rashba (solid arrows) and pure Dresselhaus (dashed arrows) SO couplings whose energy spectra are symmetrical with respect to both $k_x \to -k_x$ and $k_y \to -k_y$ transformations, leading to a high degree of cancellation of the field induced spin textures from the neighboring subbands. In Fig. 6(b) the same view is shown for the presence of both Rashba and Dresselhaus terms where the spectra are invariant only with respect to the $(k_x, k_y) \to (-k_x, -k_y)$ transformation, leading to the increasing differences in the energy dispersion shapes and creating a much smaller degree of cancellation from the neighboring subbands, thus increasing the spin texture amplitude (see

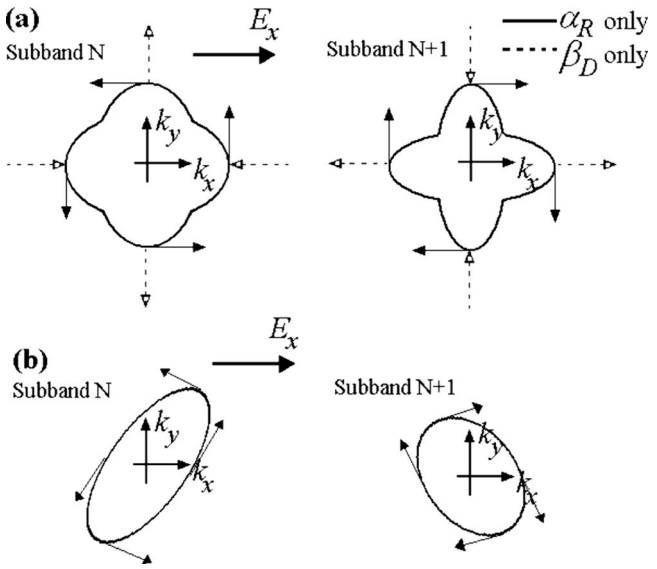

FIG. 6. (a) Schematic view of mean spin alignment for two SO-split subbands for pure Rashba (solid arrows) and pure Dresselhaus (dashed arrows) SO couplings whose energy spectra are symmetrical with respect to both $k_x \to -k_x$ and $k_y \to -k_y$ transformations, leading to a high degree of cancellation of the spin textures from the neighboring subbands induced by the electric field E_x. (b) The same as (a) for the presence of both Rashba and Dresselhaus terms where the spectra are invariant only with respect to the $(k_x, k_y) \to (-k_x, -k_y)$ transformation, leading to the increasing differences in the energy dispersion shapes and creating a much smaller degree of cancellation from the neighboring subbands, thus increasing the spin texture amplitude (see Fig. 4).

Fig. 4). The treatment of S_z component of spin textures cannot be handled in the same way since its mean value for a quantum state of our Hamiltonian is zero, meaning that the condition

$$\int_0^a S_z(x)dx = 0 \tag{9}$$

is always fulfilled. The local nonzero $S_z(x)$ component is formed by the effective magnetic field $\propto [\nabla V(x), \vec{p}]$ arising due to the superlattice potential $V(x)$. Since this potential is periodic, the mean value of its gradient is zero, which is reflected in Eq. (9). These general properties of the local nonzero $S_z(x)$ component are related only to the spatial dependence of the superlattice potential and on the applied electric field and thus they should not depend strongly on the precise value of Rashba-to-Dresselhaus ratio as long as the SO coupling is present. This expectation is consistent with the plots for $S_z(x)$ in Fig. 4(c), where the textures for three different sets of parameters are very close to each other. Since the local spin density is an actually measurable quantity in the experiments, the creation of field induced spin textures in superlattices with both Rashba and Dresselhaus SO terms should be taken into consideration for possible experimental and device purposes.

B. Variable α/β and fixed electric field

Now we shall consider the dependence of spin texture components on the ratio α/β of Rashba and Dresselhaus contributions to the SO coupling when the electric-field strength $E_x=50$ V/cm is fixed in a low-field regime of the interval in Figs. 3 and 4, which is more desirable for practical purposes. The upper limit of α/β can be estimated from the actual photocurrent experimental data[7] where in different structures constructed from different materials this ratio has been reported to vary from 1.5 to 7.6. Taking this into consideration, we shall restrict ourselves to the interval $0 \leq \alpha/\beta \leq 8.0$. Keeping all other parameters of the system unchanged, we obtain the α/β dependencies of spin texture components in a superlattice cell which are shown in Fig. 5. Point A on the α/β axis corresponds to the example of InAs-based structure with $\alpha/\beta=1.6$ considered in the previous parts of the paper, and the position of the vertical axis is displaced for a better view.

First, let us examine the lower part of the interval when $\alpha/\beta<1$, i.e., when the SO coupling is dominated by the Dresselhaus term in a macroscopically symmetrical semiconductor structure with significant BIA and negligible SIA. One can see from Fig. 5 that the only significant component of spin texture in this limit is $S_z(x)$, although it is always several times smaller in amplitude than the maximum achievable $S_x(x)$ and $S_y(x)$ components at various α/β. This local component of field induced spin texture can be nonzero since the structure has a microscopic BIA and is nonhomogeneous due to the presence of the superlattice. Nevertheless, the mean value of the out-of-plane component $S_z(x)$ is zero for all values of α/β and E_x, i.e., condition (9) is always fulfilled, as it can be checked numerically for the textures in Figs. 4(c) and 5(c).

Another important issue is the symmetry properties of the induced polarization. The presence of purely Dresselhaus SO coupling breaks the bulk inversion symmetry; i.e., the $\mathbf{r}\rightarrow-\mathbf{r}$ element of symmetry is no longer present. For the induced spin texture considered here the only component of spin is S_z, i.e., $\mathbf{S}=(0,0,S_z)$. Despite the existence of the C_2 rotation axis parallel to the x direction, the application of this rotation to the particular orientation of the induced spin $\mathbf{S}(E(x))=(0,0,S_z(E_x))$ is equivalent to the inversion $\mathbf{r}\rightarrow-\mathbf{r}$, which is no longer present as a symmetry element due to the Dresselhaus SO coupling. As for the pure Rashba coupling, the same effect is produced by the breaking of the $z\rightarrow-z$ symmetry by the SIA with the confinement potential $U(z) \neq U(-z)$. Hence, the existence of the electric-field induced S_z spin component here is consistent with the symmetry relations. It should be mentioned also that the existence of the out-of-plane spin polarization induced by the in-plane electric field in a system with both Rashba and Dresselhaus SO couplings is a well-known phenomenon in the context of the spin Hall effect where the uniformly spaced spin currents of S_z components have been predicted.[38–42]

We now consider the general case of nonzero Rashba and Dresselhaus SO terms. As we move along the α/β axis, it becomes clear that the maximum amplitudes for $S_x(x)$ and $S_y(x)$ components are achieved when Rashba and Dresselhaus terms become comparable in size, while the shape of $S_z(x)$ is only slightly modified. The $S_x(x)$ and $S_y(x)$ components both have a nonzero mean value, which is in the agreement of the calculated spin projections in Fig. 3 and is important in the scope of the practical issues of spin accumulation. The presence of both Rashba and Dresselhaus terms leads to the appearance of two nonzero components of the accumulated spin instead of one (S_y only) when the SO coupling is purely of Rashba type.[23] It should be noted that a high degree of spin polarization at equal strengths of Rashba and Dresselhaus terms is in the agreement with the results of numerous studies of transport and spin Hall phenomena in such systems. Hence, the example of $\alpha/\beta=1.6$ for InAs-based structure which was studied above in detail is promising since the desirable spin properties in such system are manifested on the highest achievable level.

Finally, let us consider the limit $\alpha \gg \beta$ when the Rashba term dominates over the Dresselhaus term, although the latter is reported still to be nonzero in practically used structures,[7] and thus the symmetry of the system on the whole α/β axis remains to be the same (except for one point $\alpha/\beta=0$). Here one can observe a nonzero integral over $S_y(x)$ only, which is consistent with previous results on the S_y component of spin accumulation in a system with pure Rashba SO coupling.[23] The $S_x(x)$ component tends to vanish, while the $S_z(x)$ component has qualitatively the same form on the whole α/β axis and zero mean value. We see that the shape and the amplitude of $S_z(x)$ are only weakly dependent on the specific value of α/β, as it has been discussed in Sec. IV A. One can see a change in the $S_z(x)$ shape occurring at the transmission trough the point $\alpha=\beta$ where the function $S_z(x)$ almost vanishes, which is in agreement with topological properties of the spin structure. However, the major part of experimentally studied nanostructures with SO coupling is characterized by some intermediate ratio α/β which is far away from any of the limiting value.[7] We believe that further theoretical and experimental studies of gated spin-orbit structures are promising since the strength of Rashba term can be widely tuned by the gate voltage,[4] and the generation of spin textures presented in Figs. 4 and 5 with different ratios α/β including the special ones seems to be experimentally accessible.

V. CONCLUSIONS

We have studied the dc charge current, the spin polarization, and the spin textures in the 1D gated superlattice with both fixed and varying Rashba and Dresselhaus SO coupling terms and the spectrum consisting of multiple pairs of spin-split minibands. We have seen how the presence of both Dresselhaus and Rashba terms with varying ratio is reflected in the SO-sensitive spin properties of the electron gas for both mean spin values and spin textures. It was found that the spin component with zero mean value can have nonvanishing field induced spin texture in a superlattice cell which

can be probed experimentally. It is shown that the consideration of the finite parameters for collision rate and temperature is nondestructive for the calculated current and spin characteristics depending on all states below the Fermi level. The knowledge of field induced spin textures in addition to the spin polarization and charge current may be instructive for both fundamental and applied issues of low-dimensional semiconductor structures with strong SO coupling.

ACKNOWLEDGMENTS

The author is grateful to V. Ya. Demikhovskii, E. Ya. Sherman, and A. A. Perov for helpful discussions. The work was supported by the RNP Program of the Ministry of Education and Science RF (Grants No. 2.1.1.2686, 2.1.1.3778, 2.2.2/4297), by the RFBR (Grant No. 09-02-1241-a), and by the USCRDF (Grant No. #BP4M01), and the Foundation "Dynasty"–ICFPM.

*khomitsky@phys.unn.ru

[1] *Semiconductor Spintronics and Quantum Computation*, Nanoscience and Technology, edited by D. D. Awschalom, D. Loss, and N. Samarth (Springer, Berlin, 2002).
[2] I. Žutić, J. Fabian, and S. Das Sarma, Rev. Mod. Phys. **76**, 323 (2004).
[3] E. I. Rashba, Fiz. Tverd. Tela (Leningrad) **2**, 1224 (1960) [Sov. Phys. Solid State **2**, 1109 (1960)]; Y. A. Bychkov and E. I. Rashba, J. Phys. C **17**, 6039 (1984).
[4] J. B. Miller, D. M. Zumbühl, C. M. Marcus, Y. B. Lyanda-Geller, D. Goldhaber-Gordon, K. Campman, and A. C. Gossard, Phys. Rev. Lett. **90**, 076807 (2003).
[5] D. Grundler, Phys. Rev. Lett. **84**, 6074 (2000).
[6] G. Dresselhaus, Phys. Rev. **100**, 580 (1955).
[7] S. Giglberger, L. E. Golub, V. V. Bel'kov, S. N. Danilov, D. Schuh, C. Gerl, F. Rohlfing, J. Stahl, W. Wegscheider, D. Weiss, W. Prettl, and S. D. Ganichev, Phys. Rev. B **75**, 035327 (2007).
[8] S. Datta and B. Das, Appl. Phys. Lett. **56**, 665 (1990).
[9] A. G. Aronov, Yu. B. Lyanda-Geller, and G. E. Pikus, Zh. Eksp. Teor. Fiz. **100**, 973 (1991) [Sov. Phys. JETP **73**, 537 (1991)].
[10] V. M. Edelstein, Solid State Commun. **73**, 233 (1990).
[11] O. E. Raichev, Phys. Rev. B **75**, 205340 (2007).
[12] S. I. Erlingsson, J. Schliemann, and D. Loss, Phys. Rev. B **71**, 035319 (2005).
[13] Z. Li and Z. Yang, Phys. Rev. B **76**, 033307 (2007).
[14] J. Yao and Z. Q. Yang, Phys. Rev. B **73**, 033314 (2006).
[15] J. Li and S.-Q. Shen, Phys. Rev. B **76**, 153302 (2007).
[16] M. Yamamoto, T. Ohtsuki, and B. Kramer, Phys. Rev. B **72**, 115321 (2005).
[17] H. Zhao, E. J. Loren, H. M. van Driel, and A. L. Smirl, Phys. Rev. Lett. **96**, 246601 (2006).
[18] J. Wang, K. S. Chan, and D. Y. Xing, Phys. Rev. B **73**, 033316 (2006).
[19] J. I. Ohe, A. Takeuchi, and G. Tatara, Phys. Rev. Lett. **99**, 266603 (2007).
[20] M. Onoda and N. Nagaosa, Phys. Rev. Lett. **96**, 066603 (2006).
[21] T. Kimura, Y. C. Otani, and P. M. Levy, Phys. Rev. Lett. **99**, 166601 (2007).
[22] R. Jansen and B. C. Min, Phys. Rev. Lett. **99**, 246604 (2007).
[23] P. Kleinert, V. V. Bryksin, and O. Bleibaum, Phys. Rev. B **72**, 195311 (2005).
[24] V. V. Bryksin and P. Kleinert, Phys. Rev. B **73**, 165313 (2006).
[25] Y. Qi, Z.-G. Yu, and M. E. Flatté, Phys. Rev. Lett. **96**, 026602 (2006).
[26] F. Zhai, K. Chang, and H. Q. Xu, Appl. Phys. Lett. **92**, 102111 (2008).
[27] M. M. Glazov and E. Ya. Sherman, Phys. Rev. B **71**, 241312(R) (2005).
[28] M.-H. Liu and C.-R. Chang, Phys. Rev. B **74**, 195314 (2006).
[29] M. Khodas, A. Shekhter, and A. M. Finkel'stein, Phys. Rev. Lett. **92**, 086602 (2004).
[30] Yu. V. Pershin, Phys. Rev. B **71**, 155317 (2005).
[31] V. Ya. Demikhovskii and D. V. Khomitsky, JETP Lett. **83**, 340 (2006) [Pis'ma Zh. Eksp. Teor. Fiz. **83**, 399 (2006)].
[32] D. V. Khomitsky, Phys. Rev. B **76**, 033404 (2007).
[33] D. V. Khomitsky, Phys. Rev. B **77**, 113313 (2008).
[34] Ali Najmaie, E. Ya. Sherman, and J. E. Sipe, Phys. Rev. Lett. **95**, 056601 (2005).
[35] J. Shi, P. Zhang, D. Xiao, and Q. Niu, Phys. Rev. Lett. **96**, 076604 (2006).
[36] N. Sugimoto, S. Onoda, S. Murakami, and N. Nagaosa, Phys. Rev. B **73**, 113305 (2006).
[37] E. I. Rashba, Phys. Rev. B **68**, 241315(R) (2003).
[38] S.-Q. Shen, Phys. Rev. B **70**, 081311(R) (2004).
[39] N. A. Sinitsyn, E. M. Hankiewicz, W. Teizer, and J. Sinova, Phys. Rev. B **70**, 081312(R) (2004).
[40] J. Li, L. Hu, and S.-Q. Shen, Phys. Rev. B **71**, 241305(R) (2005).
[41] T.-W. Chen, C.-M. Huang, and G. Y. Guo, Phys. Rev. B **73**, 235309 (2006).
[42] Y. Xing, Q.-f. Sun, and J. Wang, Phys. Rev. B **75**, 075324 (2007).